

www.aem-journal.com

# Preparation and Characterization of Ti-6-4 and Ti-8-1-1 Metal Matrix Composites with High Specific Stiffness Using Powder Hot Extrusion and Arc Remelting

Nico Moser,\* Ella Staufer, Thomas Klein, Jelena Horky, Martin Schmitz-Niederau, Erich Neubauer, Lena Trunova, and Christian Edtmaier

Titanium alloys with high stiffness are crucial for aerospace engineering and are often fabricated using additive manufacturing (AM) methods like arc or laser techniques. These high energy processes alter the microstructure and mechanical properties. To enhance stiffness, TiC and B<sub>4</sub>C are added to Ti−6Al−4V and Ti-8Al-1Mo-1V alloys via powder hot extrusion. The resulting metal matrix composites (MMCs) are analyzed in both their as-extruded and heat-treated states for microstructure and mechanical properties. To simulate an AM process, samples are remelted using a gas tungsten arc-welding (GTAW) torch and examined. In the results, it is shown that TiC and B4C increased mechanical properties up to 2 GPa cm<sup>3</sup> g<sup>-1</sup>, with the highest increase observed in heat-treated B<sub>4</sub>C samples, achieving specific stiffnesses of 34.6 GPa cm<sup>3</sup> g<sup>-1</sup> (Ti-6Al-4V) and 32.3 GPa cm $^3$  g $^{-1}$  (Ti-8Al-1Mo-1V). Powder hot extrusion proves effective in producing Ti-MMCs with high stiffness even with reactive ceramic additions. However, GTAW remelting leads to the decomposition of TiC-reinforced Ti-MMCs, significantly altering morphology and reducing stiffness below that of the base alloy.

N. Moser, E. Staufer, C. Edtmaier
Institute of Chemical Technologies and Analytics
TU Wien
A 1060 Vienna, Austria
E-mail: moser.nico@gmx.at
T. Klein
LKR Light Metals Technologies
AIT Austrian Institute of Technology
A 5282, Ranshofen, Seibersdorf, Austria
J. Horky, E. Neubauer
RHP-Technology GmbH
A 2444 Seibersdorf, Austria
M. Schmitz-Niederau, L. Trunova
voestalpine Böhler Welding Germany GmbH

Hafenstraße 21, D 59067 Hamm, Germany

The ORCID identification number(s) for the author(s) of this article can be found under https://doi.org/10.1002/adem.202400514.

© 2024 The Author(s). Advanced Engineering Materials published by Wiley-VCH GmbH. This is an open access article under the terms of the Creative Commons Attribution License, which permits use, distribution and reproduction in any medium, provided the original work is properly cited.

DOI: 10.1002/adem.202400514

# 1. Introduction

Titanium and its alloys have been established in various fields of applications throughout the last years. Especially, in the aerospace sector, the combination of lightweight and corrosion resistance has encouraged the development and improvement of titanium alloys.[1] However, since structural parts must withstand high mechanical loads in addition to being lightweight, materials with high specific stiffness and strength are of great importance. They must therefore be able to withstand high loads without deforming or even breaking and have the lowest possible density. An example of such a potential application can be found in the European Space Agency's future Athena X-ray telescope mission, where materials of highest stiffness are needed for the mirror connecting parts, as the precision of the measure-

ments depends heavily on minimizing the deformation of such components.  $\sp(2)$ 

In terms of producing such structural components, additive manufacturing (AM) provides near net-shape parts and flexibility. Currently, AM is focused on cp Ti and Ti-6-4 (Ti—6 wt% Al—4 wt% V) as the materials of choice. It has been demonstrated that Ti-6-4 can be processed by AM, either in powder or wire form. However, a vast majority of new alloys are being developed for certain niche applications, taking into account  $\alpha$  alloys,  $\beta$  alloys,  $\alpha+\beta$  alloys, as well as near- $\alpha$  alloys/near- $\beta$  alloys and even titanium aluminides. He alloy Ti-8-1-1 (Ti—8 wt% Al—1 wt% V—1 wt% Mo) alloy is known to have the highest stiffness (120 GPa) of all commercially available titanium alloys. It is classified as a near- $\alpha$  alloy containing mainly  $\alpha$ -Ti and small amounts of  $\beta$ -Ti. As improving the specific stiffness of alloys is limited, there is also the possibility of introducing reinforcing phases.

Titanium matrix composites (Ti-MMCs) combine the properties of the metallic matrix and reinforcements, mainly ceramics. The aim is to improve mechanical properties such as stiffness, strength, or creep behavior. These reinforcements can be particles or fibers, where fibers are expected to give anisotropic properties and particles can be expected to give more isotropic character to the final system. Common (particulate) reinforcements are TiC,  $B_4C$ ,  $TiB_x$ ,  $Al_2O_3$ , and SiC, where a distinction can be made

ENGINEERING

www.advancedsciencenews.com

www.aem-journal.com

between in situ and ex situ reinforcements. The former ones are classified in that way that they react with the matrix, whereas the latter do not. For example, TiC is known to be an ex situ reinforcement, because it is known—from a thermodynamic and chemical point of view—not to react with Ti, whereas B<sub>4</sub>C and SiC can react with a titanium-based matrix in the following way:[8,9]

$$5 \, \text{Ti} + \text{B}_4 \text{C} \leftrightarrow 4 \, \text{TiB} + 1 \, \text{TiC}$$
 (1)

$$Ti + SiC \leftrightarrow TiC + Si, TiC_x, Ti_5Si_3, Ti_5Si_3C_x$$
 (2)

Unfortunately, reaction products such as titanium silicide Ti<sub>5</sub>Si<sub>3</sub> or titanium carbo-silicide Ti<sub>5</sub>Si<sub>3</sub>C<sub>x</sub> have a significantly lower Young's modulus than the initial phase (SiC) and a distinctly different and usually unfavorable morphology after the reaction.<sup>[10]</sup> For example, the titanium silicide formed is needle shaped, which is much less favorable for the mechanical properties than the initial morphology of the SiC particles.<sup>[11]</sup> Other in situ reinforcement phases can result from alloying elements through the formation of intermetallic phases (IMs) such as, e.g., Ti<sub>2</sub>Cu or TiFe. However, such IMs have a significantly lower Young's modulus than ex situ phases (see Table 1). To achieve a significant increase in the Young's modulus, larger volume fractions of these IMs would therefore be required, which would usually reduce the ductility. However, specifically for Ti-8-1-1, there is another approach, namely the formation of the Ti<sub>3</sub>Al or α<sub>2</sub> phase, an ordered structure of the hexagonal  $\alpha$  phase, which is usually formed by ageing.  $^{\left[12\right]}$  A Young's modulus of 163 GPa is reported for this phase. [13]

Nevertheless, the practical implementation of the production of ex situ Ti-MMCs faces a relevant problem-controlling the reactivity of Ti with essentially all materials that can be considered as reinforcing phases (except TiBx and TiC). This is, of course, a function of temperature and time. Powder metallurgical processes are in principle a possibility, but in practice it has been shown that the usual long process times and high temperatures required lead to pronounced reactions. In addition to pressing and sintering, however, production by means of powder hot extrusion has also become established, which is particularly interesting for reactive systems, as the consolidation time can be kept very short. This was first described by Poletti et al.[14] and seemed to be an efficient way to avoid high temperatures and long process cycle times and thus effectively suppress the reactivity between Ti and ceramics like SiC. This concept was also successfully applied to other reactive systems, such as fused

Table 1. Young's modulus of Ti, Ti-6-4, Ti-8-1-1, and potential reinforcement phases.

Material	Young's modulus [GPa]	References	
Ti	100–120	[1]	
Ti-6-4	110	[1]	
Ti-8-1-1	120	[7]	
TiC	460	[36]	
TiB	550	[36]	
B <sub>4</sub> C	460	[37]	
Ti <sub>3</sub> Al	163	[12]	

tungsten carbide in Ni or Fe matrices, where the formation of a distinct and detrimental reaction layer has also been avoided.<sup>[15]</sup> When using AM methods, especially ones with high energy input such as directed energy deposition (DED) or powder bed fusion, pronounced changes in the microstructure and mechanical properties can be observed, often leading to less favorable properties.[16]

As there are no commercially available alloys other than pure Ti and Ti-6-4 in powder or wire form, we were particularly interested in the preparation of Ti-8-1-1, as well as the B<sub>4</sub>C- and TiCparticle-reinforced variants of Ti-6-4 and Ti-8-1-1 by means of powder hot extrusions, with the goal of achieving and retaining high specific stiffnesses. The focus is on the behavior of the reinforcements after a heat treatment or remelting to investigate differences in the microstructure and mechanical properties before and after a high energy impact, simulating AM. This study describes the fabrication of Ti-6-4 and Ti-8-1-1 MMCs with 3 vol% TiC or B<sub>4</sub>C via powder hot extrusion, as well as the changes occurring after heat treating and remelting. All specimens are investigated in regard of their microstructure, density. stiffness, and hardness. Results show pronounced improvements in terms of the stiffness after extrusion and in the heat-treated state. The effects of high energy impacts, as they can be expected in certain AM methods, are studied in remelted specimens and provide further insights into the complex topic of the reactions between the Ti-matrix and potential reinforcements. Changes in the mechanical properties are discussed and compared to the microstructure.

## 2. Experimental Section

All materials investigated, the Ti-6-4 as a reference, the Ti-8-1-1 alloy, and their TiC- and B<sub>4</sub>C-particle-reinforced MMC variants were prepared from the corresponding mixture of Ti Gd2 (<45 μm, Eckart TLS GmbH), Ti Gd5 (<45 μm, Eckart TLS Technik GmbH & Co), Al (<40 µm, MEPURA), and Mo ( $<5\,\mu m$ , Treibacher Industrie AG) powders. The TiC was a <45 μm powder (Alfa Products), and the B<sub>4</sub>C reinforcement was an F500 powder (equivalent to  $12.8 \pm 1 \,\mu m$ ) from 3M. In both cases, 3 vol% of reinforcement particles were added.

After mixing for 1 h, the powders were transferred into a steel capsule and welded gas tight. These capsules were then preheated for 20 min at 1000 °C (Ti-6-4) and 1100 °C (Ti-8-1-1) and extruded into rods. The extrusion ratio was 1:11, the extrusion speed was  $10 \text{ mm s}^{-1}$ , and the temperature of the recipient was 350 °C. After extrusion, the steel coating was removed and a heat treatment (1000 °C; 90 h, Ar atmosphere, slow cooling, see Figure 1) was carried out. Furthermore, as-extruded rods were gas tungsten arc-welding (GTAW) remelted with a Robacta TTW 5500, Fronius, to simulate and study their behavior during a potential wire arc melting process. The remelting was conducted using a welding current of 200 A, a 6.4 mm W electrode, and a water-cooled Cu mold. After applying a vacuum of  $6 \times 10^{-3}$  mbar, an argon purge was performed at 800 mbar overpressure. All specimens were metallographically prepared (grinding: P500, P1200, P4000; polishing: oxide polishing suspension + H<sub>2</sub>O<sub>2</sub>, etching: 1% hydrofluoric acid) perpendicular and transversal to the extrusion or building direction and

www.advancedsciencenews.com www.aem-journal.com

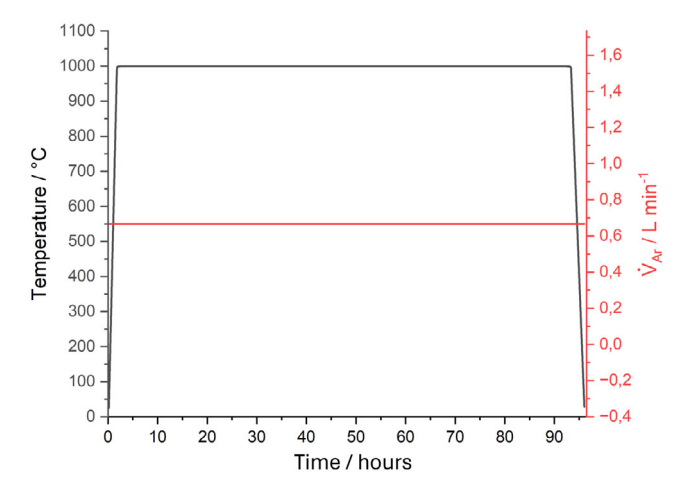
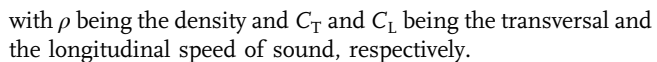


**Figure 1.** Heat-treatment cycle used for the annealing of as-extruded samples. Heating rate  $10 \, \text{K min}^{-1}$ , dwelling time  $90 \, \text{h}$ , cooling rate  $6 \, \text{K min}^{-1}$ , and argon flow  $0.67 \, \text{L min}^{-1}$ .

characterized by light microscopy (LM; Olympus GX51), scanning electron microscopy (SEM; Quanta 200 ESEM FEG from FEI), X-ray diffractometry (XRD; X'Pert MPDII), hardness (EMCO test M4U-025), density (Archimedes), and stiffness measurements. Assuming isotropic elastic properties and applying the ultrasound point analysis technique,  $^{[17-19]}$  the Young's modulus E can be calculated from Equation (3):

$$E = \rho \cdot C_{\mathrm{T}}^2 \cdot \frac{3 - 4 \cdot \left(\frac{C_{\mathrm{T}}}{C_{\mathrm{L}}}\right)^2}{1 - \left(\frac{C_{\mathrm{T}}}{C_{\mathrm{L}}}\right)^2} \tag{3}$$



Hardness values were determined with a Vickers indenter using a load of 98.1 N. Mean values from at least five individual measurements were used. Young's moduli displayed were taken from three samples.

For transmission electron microscope (TEM) imaging and selected area electron diffraction (SAED), a TECNAI F20 (acceleration voltage 200 kV) at the electron microscopy facility (university center of transmission electron microscopy [USTEM]) of TU Wien was used.

# 3. Results and Discussion

#### 3.1. Powder Hot Extrusion

#### 3.1.1. Microstructure

Figure 2 shows the microstructure of Ti-6-4 after powder hot extrusion. It is homogeneous, as it is typical for Ti-6-4 in general. The samples are fully compacted (Table 2) by the hot extrusion process and there is no visible difference in microstructure or the occurrence of pores between the longitudinal and perpendicular cross sections of the micrographs examined. A lamellar two-phase structure is observed in Ti-6-4, consisting of  $\alpha$ -Ti grains surrounded by  $\beta$ -Ti at the grain boundaries. Significant grain growth is observed after heat treatment (Figure 2c,d). The addition of 3 vol% TiC resulted in a finer microstructure, as shown in Figure 3a,c. The heat treatment leads to a clear microstructural transformation resulting in a bimodal microstructure (Figure 3c and 4c), with the TiC particles essentially

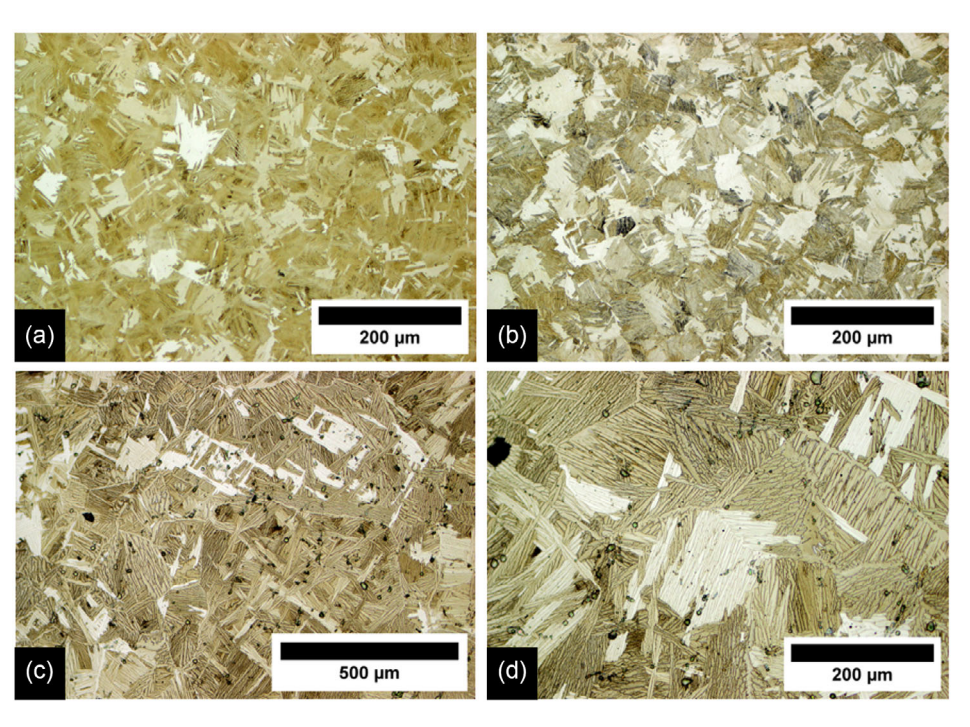


Figure 2. LM micrographs of Ti-6-4 alloy prepared via powder hot extrusion. The as-extruded samples show no differences in microstructure in a) the perpendicular and b) longitudinal cross section, respectively. c,d) The heat-treated condition at 1000 °C for 90 h. The microstructure consists of α-Ti and β-Ti.

www.advancedsciencenews.com www.aem-journal.com

Table 2. Archimedean density of as-extruded and annealed Ti-6-4, Ti-8-1-1, and MMCs

Matrix	Reinforcement	Density $[g cm^{-3}]$	
		As-extruded	Annealed 1000 °C [90 h]
Ti-6-4	_	$\textbf{4.432} \pm \textbf{0.002}$	$4.442 \pm 0.014$
Ti-6-4	3 vol% TiC	$\textbf{4.648} \pm \textbf{0.325}$	$4.418 \pm 0.003$
Ti-6-4	3 vol% B <sub>4</sub> C	$\textbf{4.383} \pm \textbf{0.001}$	$\textbf{4.424} \pm \textbf{0.006}$
Ti-8-1-1	_	$\textbf{4.367} \pm \textbf{0.001}$	$\textbf{4.345} \pm \textbf{0.013}$
Ti-8-1-1	3 vol% TiC	$\textbf{4.387} \pm \textbf{0.001}$	$\textbf{4.378} \pm \textbf{0.004}$
Ti-8-1-1	3 vol% B <sub>4</sub> C	$\textbf{4.336} \pm \textbf{0.002}$	$\textbf{4.385} \pm \textbf{0.001}$

remaining. The addition of 3 vol%  $B_4C$  has a similar refinement effect as TiC, see Figure 3b,d and 4b,d. Furthermore, a bimodal microstructure is again visible after the heat treatment, in addition to partially reacted former  $B_4C$  particles can be seen, which have a reaction zone around them from which small TiB whiskers grow out in Figure 4d.

Figure 5a,b shows the microstructure of the as-extruded Ti-8-1-1 sample. It is inhomogeneous with both, undissolved Mo- (light particles) and Al-rich (dark grey) regions. This is not surprising for Mo as the preheating temperature of 1100 °C is far from the melting point of Mo (around 2620 °C) and therefore a homogeneous distribution was not to be expected. In contrast, Al seems to have been melted and then partially distributed near the former Ti-6-4 powder particles, with lamellar  $\alpha/\beta$  regions between these areas. After the homogenization heat treatment, the microstructure changes as Mo and Al are completely dissolved and dispersed, as shown in Figure 5c,d. A somewhat bimodal

microstructure with large semi-equiaxed  $\alpha$ -grains and  $\beta$ -grain boundaries develops combined with a general grain coarsening.

In both Ti-8-1-1 MMC variants with TiC and B<sub>4</sub>C additions. the added elemental Mo and Al are again not uniformly distributed, but partially or even completely undissolved (Figure 6 and 7). Subsequent heat treatment at 1000 °C for 90 h leads to diffusion equilibrium in both compositions and thus to a homogenized microstructure in which the elements are evenly distributed (Figure 6c,d). The TiC particles show no signs of reaction either due to the hot extrusion process or after the subsequent heat treatment (Figure 6). In addition, small amounts of β-grain boundaries can be found as well as  $\beta$  areas with  $\alpha$ -lamellae inside. In contrast, significant changes can be observed after heat treatment in case of Ti-8-1-1 + 3 vol%  $B_4C$  (Figure 7c,d), although the B<sub>4</sub>C particles show stability in the as-extruded state. The microstructure shows the same features as the heat-treated Ti-8-1-1 + 3 vol% TiC sample, with the B<sub>4</sub>C particles forming both acicular titanium borides and TiC core structures with frayed titanium borides. These observed characteristic shapes of the titanium borides and/or the whisker formation from globular titanium borides found throughout all B<sub>4</sub>C MMCs are in good agreement with the literature. [20-22]

### 3.1.2. Phases

To clarify the nature of the constituent phases, XRD measurements were carried out on all samples in both the as-extruded and homogenized heat-treated states. **Figure 8** shows the diffraction patterns of all samples.

The diffraction pattern of the Ti-6-4 system in Figure 8a consists of  $\alpha$ -Ti and  $\beta$ -Ti peaks and confirms the presence of TiC, clearly showing that TiC is not altered by the manufacturing

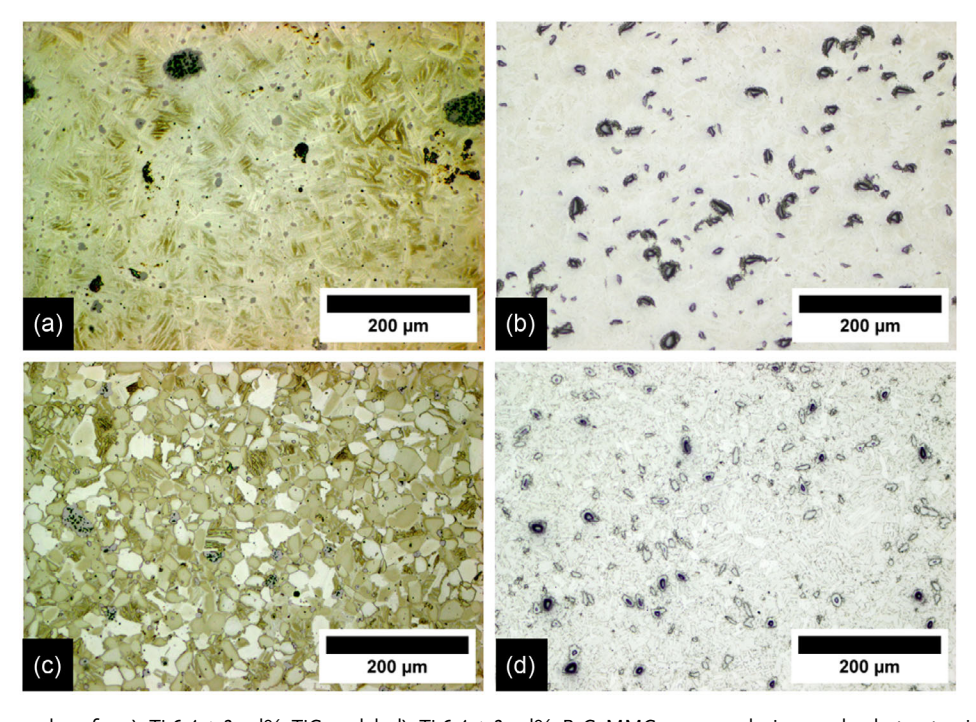


Figure 3. LM micrographs of a,c) Ti-6-4 + 3 vol% TiC and b,d) Ti-6-4 + 3 vol%  $B_4C$  MMCs prepared via powder hot extrusion and heat-treated (1000 °C for 90 h).

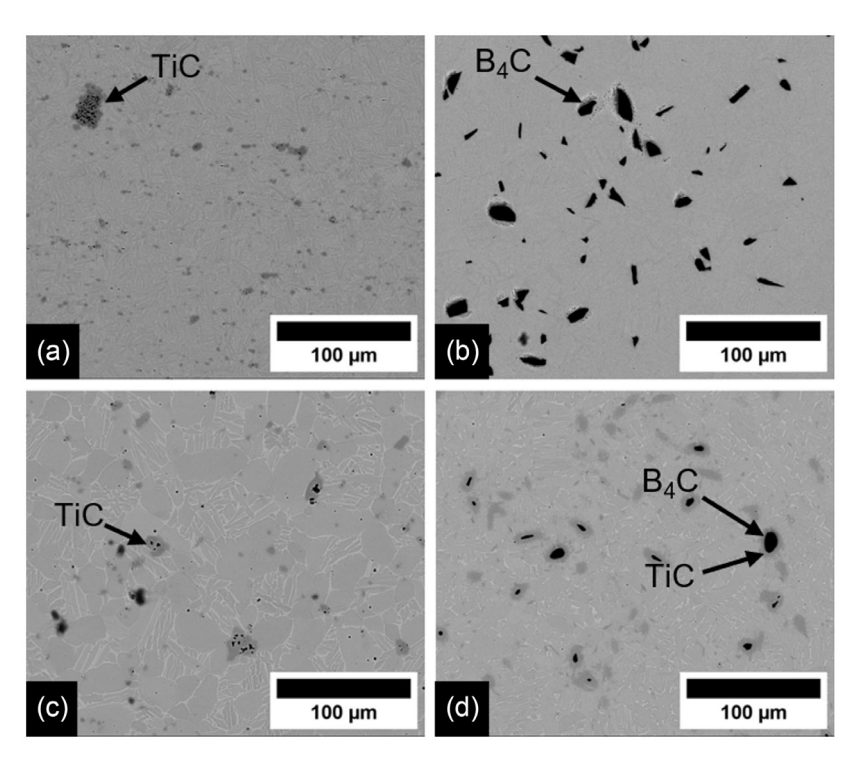
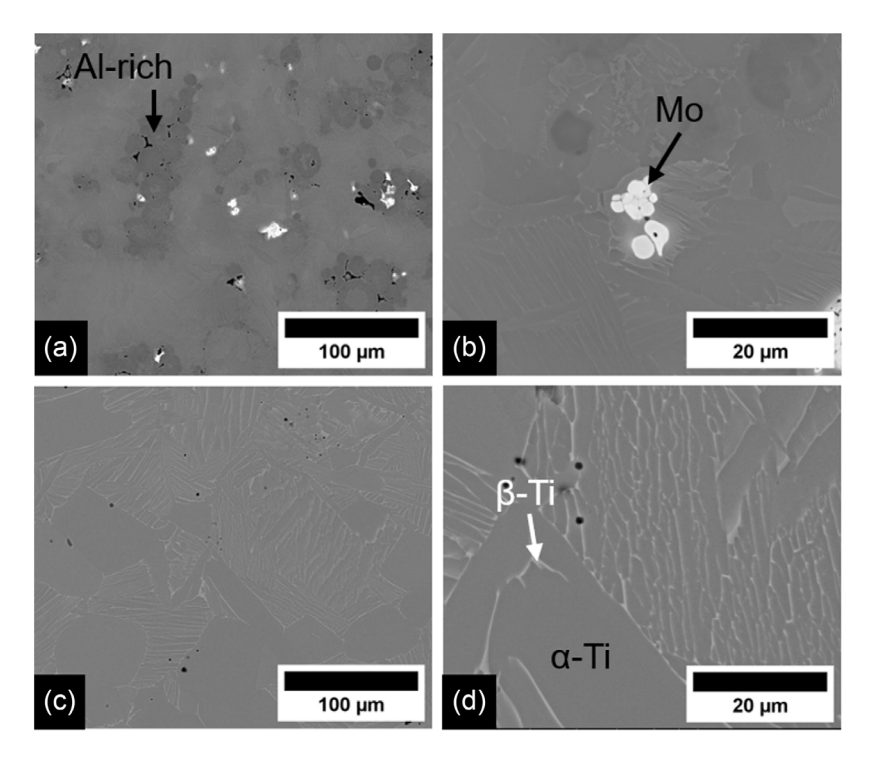


Figure 4. SEM micrographs of a,c) Ti-6-4 + 3 vol% TiC and b,d) Ti-6-4 + 3 vol%  $B_4C$  MMCs prepared via powder hot extrusion. c,d) The heat-treated condition (1000 °C for 90 h) indicates that  $B_4C$  has—at least partially—reacted to TiC and TiB, whereas TiC is not affected by the heat treatment. The black components are the used carbides TiC and  $B_4C$ .



**Figure 5.** SEM micrographs of Ti-8-1-1 alloy prepared via powder hot extrusion. a,b) The as-extruded samples show undissolved Mo particles (light) and Al-rich areas (dark grey). c,d) After the heat treatment (1000 °C for 90 h), a homogenous two-phase microstructure, consisting of α-Ti (grey) and β-Ti (light), is obtained.

www.aem-journal.com

www.advancedsciencenews.com

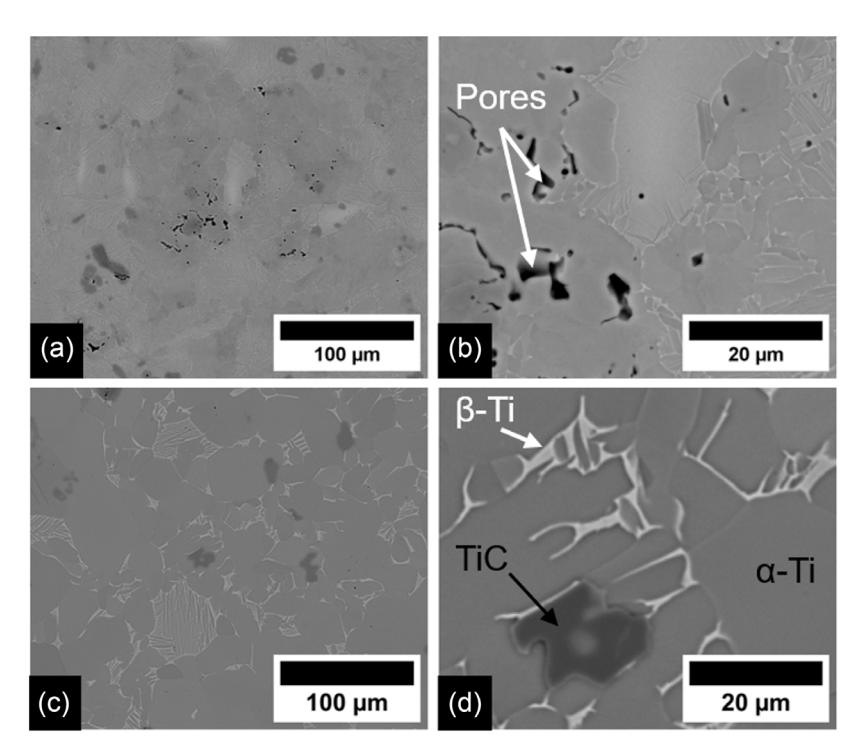


Figure 6. SEM micrographs of Ti-8-1-1 + 3 vol% TiC MMC prepared via powder hot extrusion. a,b) The as-extruded samples show Mo-rich areas (lighter areas) and minor porosity. c,d) After the heat treatment at 1000 °C for 90 h a bimodal microstructure is obtained while the TiC particles (dark grey) remain in their shape.

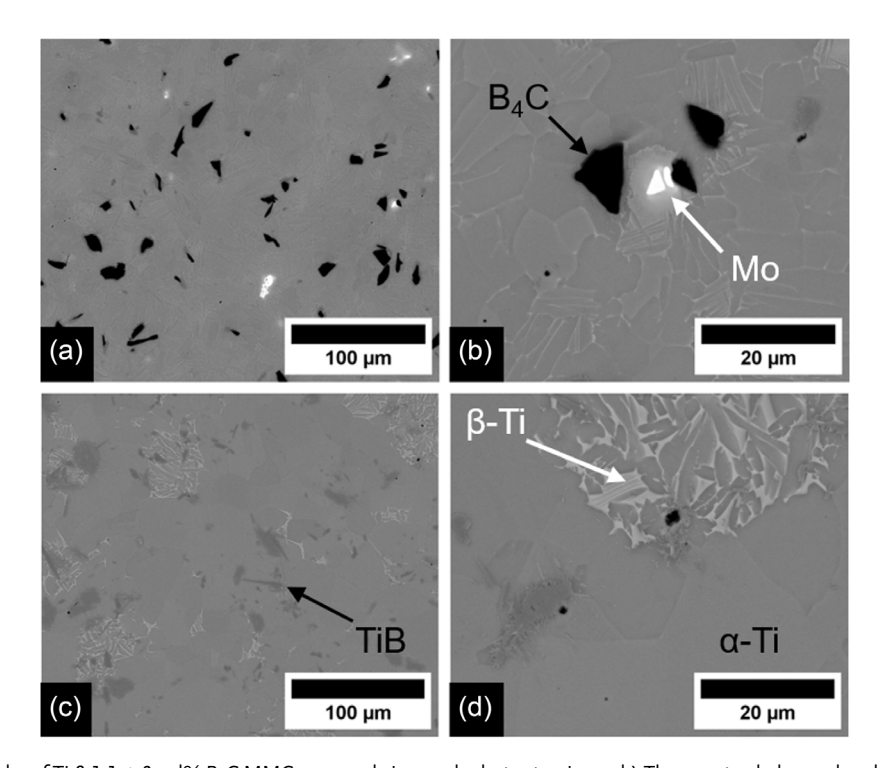


Figure 7. SEM micrographs of Ti-8-1-1 + 3 vol%  $B_4$ C MMC prepared via powder hot extrusion. a,b) The as-extruded samples show Mo-rich areas (bright) and completely unreacted  $B_4$ C (black). c,d) After the heat treatment at 1000 °C for 90 h, the Mo is completely dissolved and  $B_4$ C has reacted to TiC and TiB. The microstructure is bimodal containing α-Ti with almost no β-Ti grain boundaries and β-Ti regions.

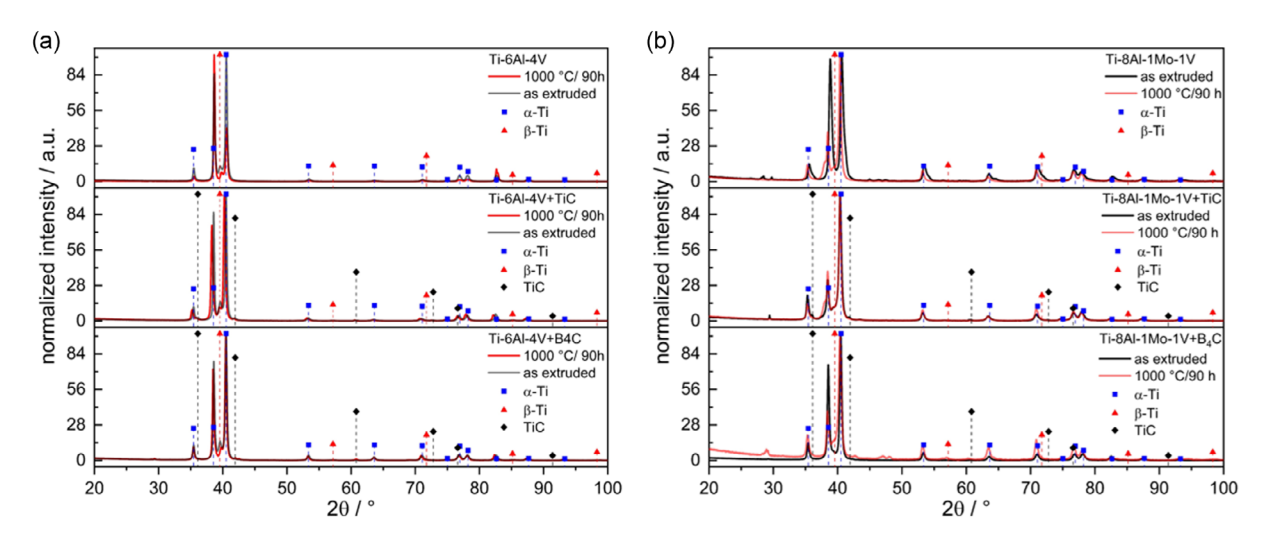


Figure 8. XRD pattern of a) Ti-6-4 and b) Ti-8-1-1 with and without TiC and B<sub>4</sub>C particle reinforcement. The presence of  $\alpha$  and  $\beta$  phase is confirmed throughout all samples.

process. Although B<sub>4</sub>C could not be clearly identified either in the as-extruded or heat-treated state, due to the overlap with the  $\alpha$ -Ti diffraction peak, the pattern of TiC, which is only visible in the heat-treated state, is an indicator of the reaction of B<sub>4</sub>C.

The  $\alpha$  phase and  $\beta$  phase can be identified throughout all Ti-8-1-1 samples, which is in accordance with the observed microstructure. In both, the as-extruded and heat-treated states, the presence of TiC can also be verified, but the as-extruded Ti-8-1-1 + 3 vol% B<sub>4</sub>C sample shows no B<sub>4</sub>C peaks at all, due to the overlap with  $\alpha$ -Ti. Therefore, the presence of TiC peaks again confirms the reaction of B<sub>4</sub>C to TiC and TiB observed in the microstructure. A small peak at 29° 2θ implies the presence of the  $\alpha_2$  (Ti<sub>2</sub>Al) phase in the Ti-8-1-1 samples, which was not found in the particle-reinforced samples, see Figure 8b.

To confirm the presence of the  $\alpha_2$  phase, a heat-treated Ti-8-1-1 sample was characterized by TEM and SAED, see Figure 9. The TEM dark-field micrograph in Figure 9a shows a dark area representing a  $\beta$  grain and a speckled area representing an  $\alpha$ grain. The SAED pattern from the  $\alpha$  grain is shown in Figure 9b. It is noteworthy, that two spots can be found for the  $10\overline{1}1$  direction. The one closer to the central spot belongs to the  $\alpha_2$  phase's superstructure, the other one to the  $\alpha$  phase. The measured interplanar distances for both points are 3.407 Å ( $\alpha_2$ ) and 2.252 Å ( $\alpha$ ), thus clearly confirming the presence of the  $\alpha_2$  phase, which is classified as an ordered structure of the  $\alpha$  phase. The  $\alpha_2$  phase was found only within regions of the  $\alpha$ grains, consistent with its formation because of short-range diffusional redistribution. The measured interplanar distances are in good agreement with the results of other researchers, who experimentally obtained 3.515 Å ( $\alpha_2$ ) and 2.224 Å ( $\alpha$ ) for the 1011 direction.<sup>[23]</sup>

# 3.1.3. Hardness and Elastic Properties

The hardness of Ti-6-4, both in the as-extruded and the heattreated state (Table 3), agrees well with typical hardness values of around 320 HV10 reported in the literature. [24] The addition

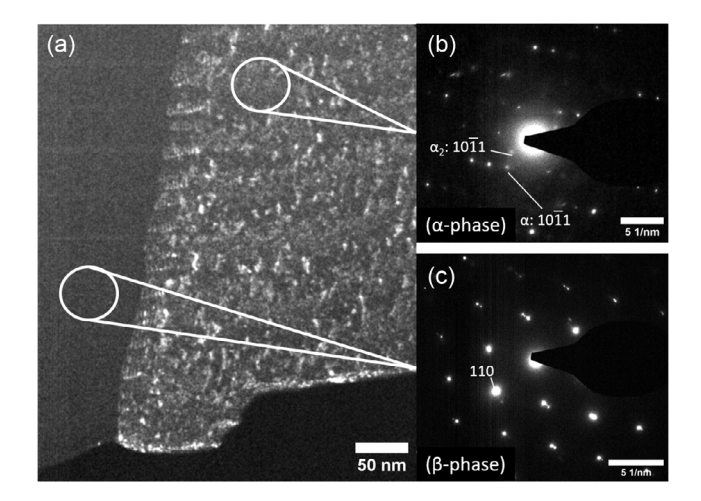


Figure 9. a) TEM dark-field micrograph of the heat-treated Ti-8-1-1 sample, displaying a  $\alpha$ -grain and  $\beta$ -grain boundary with the corresponding SAED of b) the  $\alpha$  phase and c)  $\beta$  phase. In the  $\alpha$  phase, the interplanar distance of the  $10\overline{1}1$  reflection appears for both  $\alpha$  and  $\alpha_2$  with a significant difference 2.252 Å ( $\alpha$ ) and 3.407 Å ( $\alpha_2$ ).

Table 3. Vickers hardness HV10 of as-extruded and annealed Ti-6-4, Ti-8-1-1, and MMCs.

Matrix	Reinforcement		Hardness [HV10]		
		As extruded	Heat-treated at 1000 °C [90 h]		
Ti-6-4	_	$\textbf{313} \pm \textbf{6}$	$320\pm5$		
Ti-6-4	3 vol% TiC	$335 \pm 10$	$356\pm2$		
Ti-6-4	3 vol% B <sub>4</sub> C	$\textbf{354} \pm \textbf{25}$	$\textbf{429} \pm \textbf{3}$		
Ti-8-1-1	-	$\textbf{284} \pm \textbf{9}$	$\textbf{303} \pm \textbf{5}$		
Ti-8-1-1	3 vol% TiC	$\textbf{377} \pm \textbf{8}$	$394 \pm 10$		
Ti-8-1-1	3 vol% B <sub>4</sub> C	$\textbf{367} \pm \textbf{9}$	$\textbf{422} \pm \textbf{8}$		

www.advancedsciencenews.com www.aem-journal.com

of both TiC and  $B_4C$  leads to an increase in hardness compared to the unreinforced Ti-6-4, with this being particularly pronounced in the case of the heat-treated  $B_4C$  MMCs due to the reaction to titanium borides.

Interestingly, the unreinforced Ti-8-1-1 has a lower hardness than Ti-6-4. In the as-extruded state, this is clearly because the added Mo and Al are not completely dissolved and thus the matrix does not represent the nominal composition of Ti-8-1-1. Although the heat treatment increases the hardness as expected due to the homogenization of Al and Mo, this heat-treated and homogenized sample also has a lower hardness than Ti-6-4. This could be due to the different  $\alpha/\beta$  microstructural proportions. The addition of ceramic particles leads to an almost equal increase in hardness in both cases, as-extruded and heat-treated.

The results of the Young's modulus measurements are given in **Table 4**. The Young's modulus of the Ti-6-4 reference sample is of about 117.7 GPa in the as-extruded state and about 118.9 GPa for the heat-treated state, which is in good agreement with the values of about 107-122 GPa reported in the literature by commercial manufacturers. [25] As expected, the heat treatment has no significant effect on the Young's modulus (Table 4). However, due to the particle reinforcement, a significant increase in the Young's modulus can be observed compared to the unreinforced variant. In particular, the heat-treated sample with the addition of B<sub>4</sub>C shows a significantly high stiffness of 153.1 GPacorresponding to a specific stiffness of  $34.6\,\mathrm{GPa}\,(\mathrm{g\ cm^{-3}})^{-1}$ , which can be attributed to the formation of TiB and TiC (see Equation (1)), where potentially 4 mol TiB can be formed from 1 mol B<sub>4</sub>C, leading to a higher quantity of stiffer TiB, resulting in an overall higher stiffness.

Two key observations can be made for the Ti-8-1-1 series:

Table 4. (Specific) Young's modulus of as-extruded and annealed Ti-6-4, Ti-8-1-1, and MMCs.

Matrix	Reinforcement	Young's modulus [GPa]		Specific ` modulus [GI	
		As-extruded	Annealed	As-extruded	Annealed
Ti-6-4	-	$\textbf{117.7} \pm \textbf{0.5}$	$\textbf{118.9} \pm \textbf{0.6}$	$26.6 \pm 0.1$	$26.8 \pm 0.1$
Ti-6-4	3 vol% TiC	$\textbf{128.2} \pm \textbf{9.2}$	$\textbf{122.2} \pm \textbf{3.5}$	$\textbf{27.6} \pm \textbf{0.1}$	$\textbf{27.7} \pm \textbf{0.8}$
Ti-6-4	3 vol% B <sub>4</sub> C	$124.0\pm0.9$	$\textbf{153.1} \pm \textbf{3.5}$	$28.3 \pm 0.2$	$\textbf{34.6} \pm \textbf{0.8}$
Ti-8-1-1	_	$\textbf{122.5} \pm \textbf{1.5}$	$\textbf{133.2} \pm \textbf{1.1}$	$28.1 \pm 0.3$	$\textbf{30.7} \pm \textbf{0.2}$
Ti-8-1-1	3 vol% TiC	$142.4\pm1.7$	$144.4 \pm 2.0$	$\textbf{32.5} \pm \textbf{0.4}$	$33.0 \pm 0.4$
Ti-8-1-1	3 vol% B <sub>4</sub> C	$\textbf{131.9} \pm \textbf{1.3}$	$\textbf{141.4} \pm \textbf{0.7}$	$\textbf{30.4} \pm \textbf{0.3}$	$\textbf{32.3} \pm \textbf{0.2}$

First, the unreinforced as-extruded Ti-8-1-1 alloy has a relatively low Young's modulus of 122.5 GPa compared to a commercial supplier's reference. A duplex annealed 898 °C/1 h/air-cooled and 593 °C/24 h/air-cooled Ti-8-1-1 alloy is stated to have a Young's modulus of 135 GPa. This was to be expected given that the as-extruded state is an inhomogeneous one where the alloying elements are not in solid solution. There is therefore a significant difference between the as-extruded and heat-treated states, resulting in a Young's modulus of 133.5 GPa for the later.

Second, the addition of particles to the Ti-8-1-1 alloy results in a significant increase in stiffness, with Ti-8-1-1 + 3 vol% TiC exhibiting a Young's modulus as high as 142.4 GPa. Heat treatment affects both the Ti-8-1-1 and Ti-8-1-1 + 3 vol%  $B_4C$  samples, leading to an increase of about 10 GPa for both. For the unreinforced Ti-8-1-1, it can be assumed that the reasons for this increase are the solid solution of undissolved alloying elements and the formation of the  $\alpha_2$  phase. A similar pattern is observed in the hardness measurements shown in Table 3. Particle reinforcement results in an increase in hardness of 80–90 HV10. Heat-treatment results in a small increase for Ti-8-1-1 and Ti-8-1-1 + 3 vol% TiC. However, a significant increase is observed in the sample Ti-8-1-1 + 3 vol%  $B_4C$  after the heat treatment, which is due to the  $B_4C$  reaction.

# 3.2. GTAW Remelting

#### 3.2.1. Microstructure

In **Figure 10**, a piece of an extruded rod (Figure 10a) and the MMC after the GTAW remelting (Figure 10b) are shown. The steel capsule of the rod has been removed by turning to avoid contamination in the melting process. The melted sample itself shows some shrinking cavities.

The microstructures of Ti-6-4 and Ti-8-1-1 MMCs processed in this way are shown in **Figure 11** and **12**. The GTAW remelted Ti-6-4 sample (Figure 11a) exhibits an  $\alpha/\beta$  and martensitic microstructure. The addition of TiC (Figure 11b,c) leads to a significant change in the microstructure after melting. The former TiC particles appear to have dissolved and precipitated as dendrites or needles. Moreover, no  $\alpha/\beta$  structure is visible and the matrix appears to be single phase.

By comparing Figure 11 and 12 with Figure 4, 6, and 7, one can see that the morphology of the TiC and B<sub>4</sub>C particles changes significantly due to melting during the GTAW process. In the case of B<sub>4</sub>C, this is expected due to the chemical instability and the associated formation of Ti borides, whereas TiC should





Figure 10. MMC after powder hot extrusion and removal of a) the steel capsule and b) MMC after GTAW remelting.

**4DVANCED** 

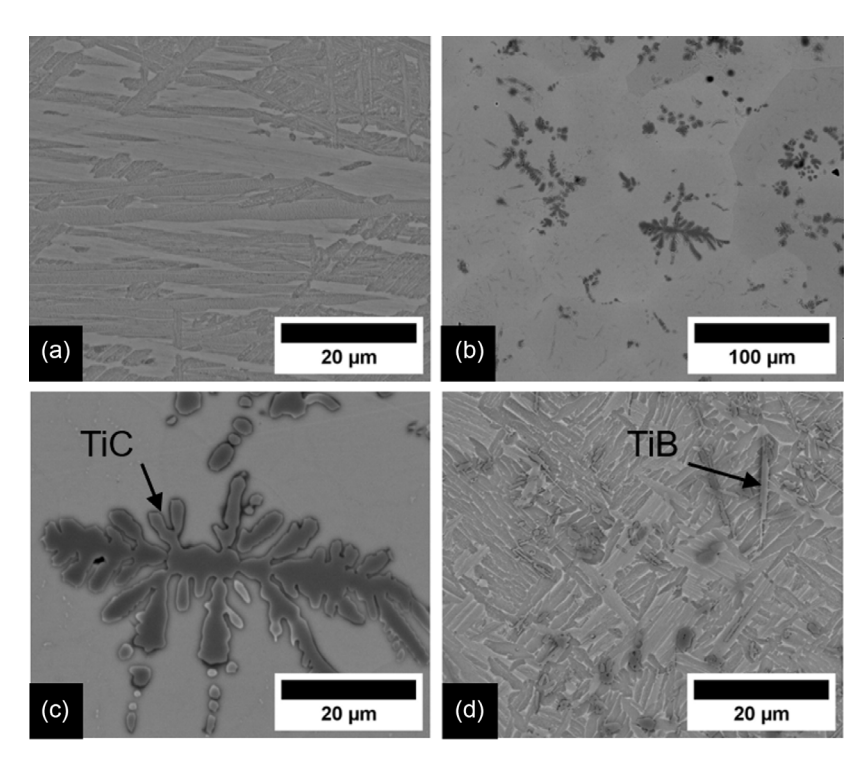


Figure 11. SEM micrographs of Ti-6-4 alloy and MMCs prepared by GTAW remelting of hot extruded rods. a) The alloy without reinforcement shows a lamellar structure. b,c) The remelted Ti-6-4 + 3 vol% TiC sample shows dendritic TiC precipitates, while an  $\alpha/\beta$  structure typical for Ti-6-4 is absent. d) The remelted Ti-6-4 + 3 vol% B<sub>4</sub>C sample shows a coarse lamellar structure without original B<sub>4</sub>C particles as they have reacted to form TiC and TiB.

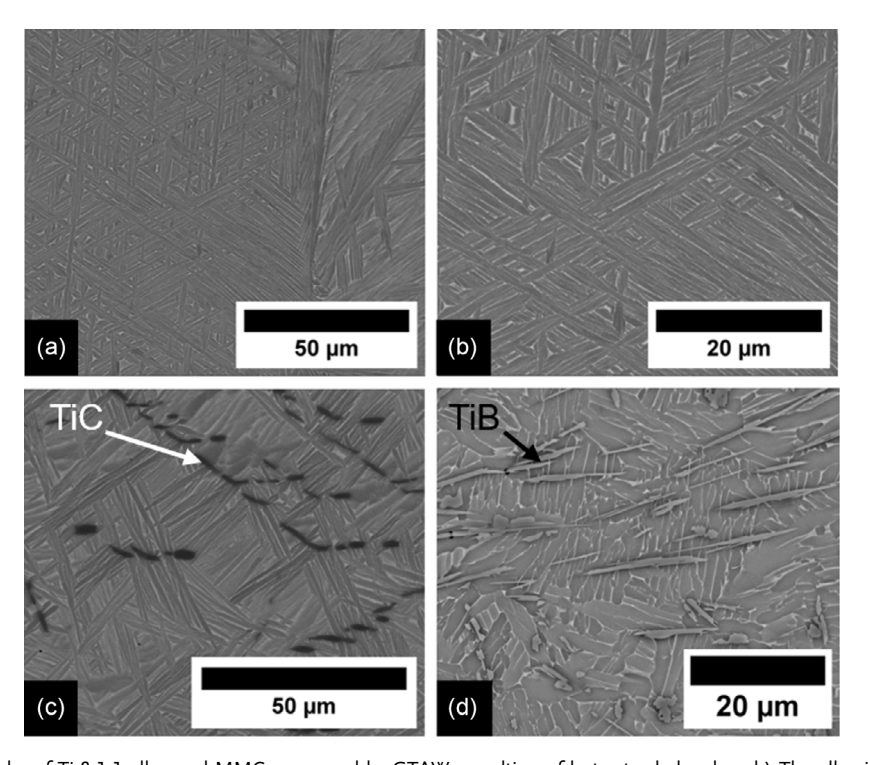


Figure 12. SEM micrographs of Ti-8-1-1 alloy and MMCs prepared by GTAW remelting of hot extruded rods. a,b) The alloy itself shows prior-β grains with a Widmannstätten structure inside. c) The remelted Ti-8-1-1 + 3 vol% TiC sample (c) shows no TiC particles in their original shape; these appear to have reacted during the melting process and precipitated in a dispersed filamentary morphology. The Widmannstätten structure is preserved. d) The Ti-8-1-1 + 3 vol%  $B_4C$  sample shows a coarse lamellar structure without original  $B_4C$  particles that reacted to form TiC and TiB.

www.aem-journal.com

be nonreactive and inert toward Ti. However, it appears that the particularly high temperature in the GTAW leads to a decomposition or melting of the TiC (melting point  $\approx\!3160\,^\circ\text{C}$ ). On cooling, TiC precipitates again, but apparently in a different morphology.

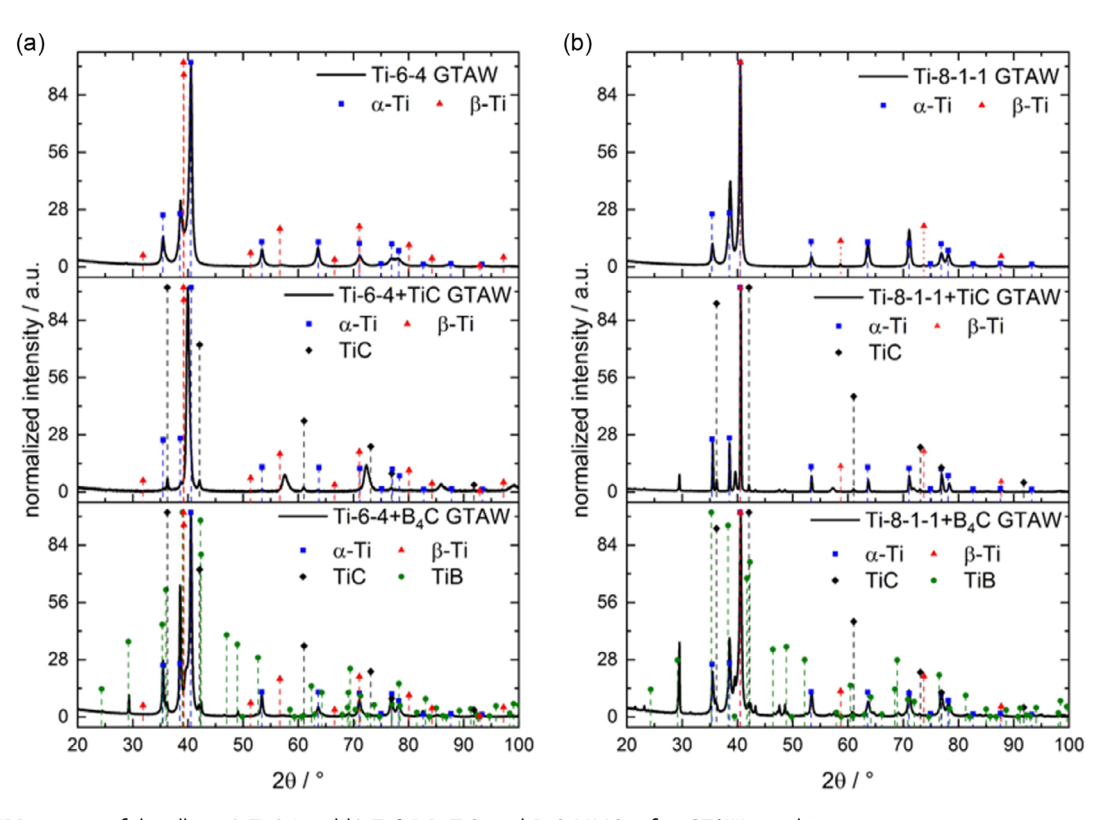
This has also been observed during laser cladding of TiC and Inconel 718 powder mixtures on an AISI 304 substrate. [27] In these investigations, the melting temperature of TiC is not reached, but a melt pool is formed from the Inconel and AISI substrate in which the TiC can dissolve and is precipitate again during cooling. This dissolution in the melt pool is clearly time dependent, i.e., the shorter the duration of a melt pool formation, the greater the probability that the TiC will remain in its original morphology. By decreasing the laser scanning speed, the melt pool lifetime and the solidification shelf time increase while the cooling rate decreases, leading to an increasing dissolution of the TiC particles and eventually to a complete decomposition/dissolution of the TiC particles. Dendritic structures can then be observed during cooling and reprecipitation, modifying the chemical and mechanical properties of the matrix. Another study observed similar microstructural changes in laser-metaldeposited TiC on Inconel 718, resulting in the formation of a (Ti,M)C (M = Nb and Mo) carbide interfacial layer, as well as dendritic structures formed during solidification of fully molten and precipitated TiC particles. [28] The microstructure and morphology of TiC after the GTAW remelting shown in Figure 12 are also consistent with the microstructural observations made by other researchers in the preparation of Ti-C-N to investigate the influence of nitrogen on the formation and morphology of TiC by the arc-melting method. [29] The authors observed a change in the microstructure of the TiC particles formed as the amount of nitrogen increased. Other similar observations have been made during selective laser melting of Ti-6-4 with TiC additions. [30–33] Similar in situ precipitation reactions of carbides have previously been reported to occur in C-alloyed titanium aluminides after heat treatment in the  $\beta$ -single-phase region. [34]

#### 3.2.2. Phases

The diffraction patterns of Ti-6-4 and Ti-8-1-1 processed with GTAW are shown in **Figure 13**. The samples without reinforcements result in the usual  $\alpha/\beta$  patterns for Ti-6-4 (Figure 13a) and Ti-8-1-1 (Figure 13b). The two TiC variants both clearly show reflexes for TiC, while the  $B_4C$  samples again show that no  $B_4C$  is present, but rather the reaction products TiC and TiB. Interestingly, when comparing the unreinforced Ti-6-4 sample and the Ti-6-4 + TiC sample, it is noticeable that there is an alternation between the  $\alpha$ -Ti and  $\beta$ -Ti contents. The Ti-6-4 + TiC sample shows almost exclusively  $\beta$ -Ti, whereas the unreinforced sample shows  $\alpha/\beta$ -Ti peaks. These findings are also in good agreement with the microstructure observed in Figure 11b,c. This is most likely due to the decomposition of the TiC during GTAW remelting, where C can also dissolve into Ti, which is also supported by a phase shift in the XRD pattern shown in Figure 13b.  $^{[35]}$ 

# 3.2.3. Hardness and Elastic Properties

The hardness and Young's moduli of the different materials processed by GTAW remelting are presented in Table 5.



 $\textbf{Figure 13.} \ \, \text{XRD pattern of the alloys a) Ti-6-4 and b)} \ \, \text{Ti-8-1-1, TiC, and B$_{4}$C MMCs after GTAW remelting.}$ 

ADVANCED ENGINEERING MATERIALS

www.advancedsciencenews.com www.aem-journal.com

**Table 5.** Hardness HV10 and Young's modulus of GTAW-processed Ti-6-4, Ti-8-1-1, and their MMCs.

Matrix	Reinforcement	Hardness [HV10]	Young's modulus [GPa]	Specific Young's modulus [GPa cm³ g <sup>-1</sup> ]
Ti-6-4	-	$\textbf{362} \pm \textbf{7}$	118	26.9
Ti-6-4	3 vol% TiC	$\textbf{464} \pm \textbf{8}$	104	22.2
Ti-6-4	3 vol% B <sub>4</sub> C	$409 \pm 4$	127	28.8
Ti-8-1-1	_	$\textbf{293} \pm \textbf{20}$	125	28.9
Ti-8-1-1	3 vol% TiC	$\textbf{395} \pm \textbf{20}$	117	26.9
Ti-8-1-1	3 vol% B <sub>4</sub> C	$428\pm3$	130	30.0

The hardness of the GTAW-processed materials shows a similar trend to that of the extruded samples: on the one hand, the hardness of Ti-8-1-1 is lower than that of Ti-6-4, indicating different  $\alpha/\beta$ -phase ratios between the two materials; on the other hand, the presence of TiC or B<sub>4</sub>C significantly increases the hardness compared to the unreinforced variant. However, a direct comparison of the hardness values between the extruded samples and the GTAW samples shows that the hardness of Ti-6-4 after TIG is about 40 HV10 higher than in the heat-treated extruded state. The Ti-6-4 + 3 vol% TiC sample is also significantly harder after GTAW than after extrusion and heat treatment, whereas the hardness of the Ti-6-4 + 3 vol% B<sub>4</sub>C sample is slightly lower after GTAW remelting. These differences between the two processing methods are seen in the Ti-8-1-1 sample, where the hardness after GTAW is comparable to the hardness after extrusion and heat treatment.

In terms of Young's modulus, the results after GTAW remelting are like those after hot extrusion and heat treatment in the case of unreinforced Ti-6-4 and to some extent also in the case of unreinforced Ti-8-1-1. However, there is a clear discrepancy between GTAW and extrusion for the reinforced variants: both Ti-6-4 and Ti-8-1-1 with TiC or B<sub>4</sub>C have a significantly lower Young's modulus after TIG than their counterparts in the heat-treated extruded state (Please note that due to the small sample volumes, the measurements of Young's modulus after GTAW processing were only possible on single samples in contrast to the measurements on the extruded samples, where the measurements were carried out on three samples in each case. The reliability of the measured results and their interpretation is therefore sometimes limited, but at least the trends are recognizable).

Based on these results, one can see that the difference in hardness of Ti-6-4 between the GTAW remelted and the hot extruded and heat-treated sample may be due to their different heat-treatment conditions and different proportions of  $\alpha/\beta$ . Furthermore, the difference in the case of Ti-6-4 + 3 vol% TiC between the two conditions can also be attributed to the decomposition of the TiC and the formation of a significantly different morphology of the reformed TiC particles compared to the original unreacted ones and attributed to dissolved C in Ti. Although, C has a vanishingly low equilibrium concentration in  $\alpha$ -Ti at room temperature, its solubility is pronounced at higher temperatures and in  $\beta$ -Ti. Since the cooling rate during GTAW remelting is not known in detail but can be assumed to be very high, it is very likely that higher nonequilibrium levels of carbon are present in the titanium lattice, which may contribute to a hardening effect.

However, this difference in hardness should also occur with the Ti-8-1-1 + 3 vol% TiC, but this is not apparent. This may be due to the significantly different size of the reformed TiC particles after GTAW remelting, as their size is significantly larger in case for Ti-6-4 + 3 vol% TiC than for Ti-8-1-1 + 3 vol% TiC and the morphology is also significantly different, which is dendritic-shaped TiC in the case of Ti-6-4 and filament-like in the case of Ti-8-1-1.

The differences in the results of the Young's modulus between the GTAW samples and the hot extruded heat-treated samples may also be due to the different sizes and morphologies of the TiC or  $B_4C$  particles or their reaction products. This change of mechanical properties has been previously reported for  $Ti_5Si_3$ .<sup>[10]</sup>

## 4. Conclusion

The investigations presented in this article have shown that powder hot extrusion is a versatile method of producing Ti alloys such as Ti-6-4 and Ti-8-1-1, as well as their MMCs. However, in the case of Ti-8-1-1, it is necessary to apply a subsequent heat treatment to obtain a homogeneous distribution of alloying elements such as Al and high melting alloying elements such as Mo, which are added in elemental form.

It is shown that particle reinforcement of Ti-8-1-1 with TiC and  $B_4C$  leads to an increase in stiffness and hardness in the asextruded state. Subsequent heat treatment affects the Ti-8-1-1 alloy and the Ti-8-1-1 + 3 vol%  $B_4C$  MMC, resulting in increased stiffness in both cases. For Ti-8-1-1, this is explained by the formation of the  $\alpha_2$  phase during heat treatment, resulting in an increase in Young's modulus from up to 133.2 GPa, because of the higher intrinsic stiffness of the intermetallic. In the case of Ti-8-1-1 + 3 vol%  $B_4C$  MMC, the reaction of  $B_4C$  to TiC and TiB is the dominant factor, resulting in an increase up to 141.4 GPa, due to the higher intrinsic stiffness of the in situ formed TiB.

The GTAW remelting studies showed a decomposition effect for the TiC-reinforced Ti-6-4 and Ti-8-1-1 MMCs, resulting in a significant change in the microstructure. This resulted in significantly lower Young's moduli compared to extruded and heattreated materials.

The results presented provide fundamental knowledge for assessing the applicability of ceramic reinforcements in titanium alloys with respect to their processing conditions. For powder-based AM methods, the proposed MMCs and their behavior during WA-DED may be resulting in further research; on these materials, especially experiments minimizing the high energy inputs may lead to a more controlled microstructure and minimize the chance of reactions of the reinforcing particles. The nature of the interaction between Ti alloys and TiC may also be studied in terms of thermal analysis and/or quenching experiments.

# Acknowledgements

This research has been funded by the Austrian Federal Ministry for Climate Action, Environment, Energy, Mobility, Innovation, and Technology (BMK) within the "Austrian Space Applications Program, ASAP" in the project

**ADVANCED** SCIENCE NEWS. ENGINEERING

www.advancedsciencenews.com www.aem-journal.com

"Ti4Space – Optimized Titanium Alloys for Space Applications Processed by Directed Energy Deposition" (grant agreement no. 885338) administered by FFG. The authors also acknowledge the University Centre of Transmission Electron Microscopy (USTEM) at TU Wien for providing their TEM facilities. The authors acknowledge TU Wien Bibliothek for financial support through its Open Access Funding Programme.

# **Conflict of Interest**

The authors declare no conflict of interest.

# **Data Availability Statement**

The data that support the findings of this study are available from the corresponding author upon reasonable request.

# **Keywords**

additive manufacturings, extrusions, metal-matrix composites (MMCs), phase stabilities, powder processings, stiffnesses

Received: February 28, 2024 Revised: May 17, 2024 Published online:

- [1] C. Leyens, M. Peters, in *Titanium and Titanium Alloys*, WILEY-VCH Verlag GmbH and Co. KGaA, Weinheim **2003**.
- [2] K. Nandra, X. Barcons, J.-W. den Herder, M. Watson, D. Barret, A. Fabian, L. Piro, Athena: The Advanced Telescope for High-Energy Astrophysics, Volker Springel, Garching 2015.
- [3] B. Dutta, F. Froes, The Additive Manufacturing (AM) of titanium alloys, Metal Powder Report, Vol. 72, 2017, p. 96.
- [4] S. A. Etesami, B. Fotovvati, E. Asadi, J. Alloys Compd. 2022, 895, 162618.
- [5] W. Wu, M. Brandt, S. Sun, J. Elambasseril, Q. Liu, K. Latham, K. Xia, M. Qian, *Acta Mater.* 2015, 85, 74.
- [6] V. Anil Kumar, R. Gupta, M. Prasad, S. Narayana Murty, J. Mater. Res. 2021, 36, 689.
- [7] R. Boyer, G. Welsch, E. Collings, in Materials Properties Handbook: Titanium Alloys, Vol. 1, ASM International, Ohio 1994.
- [8] D. Ni, L. Geng, J. Zhang, Z. Zheng, Scr. Mater. 2006, 55, 429.
- [9] B. Kool, M. Kabel, A. Kloosterman, J. De Hosson, *Acta Mater.* 1999, 47, 3105.
- [10] R. Mitra, N. Prasad, Y. Mahajan, Trans. Indian Inst. Met. 2008, 61, 427.

- [11] P. Krakhmalev, I. Yadroitsev, Intermetallics 2014, 46, 147.
- [12] A. Fitzner, L. Prakash, J. Quinta da Fonseca, M. Thomas, S.-Y. Zhang, J. Kelleher, P. Manuel, M. Preuss, Acta Mater. 2016, 103, 341.
- [13] H. Liu, K. Tong, X. Feng, B. Wen, Intermetallics 2021, 139, 107368.
- [14] C. Poletti, M. Balog, T. Schubert, V. Liedtke, C. Edtmaier, Compos. Sci. Technol. 2008, 68, 2171.
- [15] C. Edtmaier, World PM2016 Refractory Materials II, European Powder Metallurgy Association, Hamburg 2016.
- [16] S. Jing, W. Yachao, I. Mater. Sci. 2020, 55, 9883.
- [17] A. Migliori, J. Maynard, Rev. Sci. Instrum. 2005, 76, 121301.
- [18] R. Brennan, M. Golt, M. Ivill, Comparison of Dynamic Methods for Determining Elastic Property Measurements of Solid Materials, Weapons and Materials Research Directorate, DEVCOM Army Research Laboratory 2020.
- [19] M. Radovic, E. Lara-Curzio, L. Riester, Mater. Sci. Eng. A 2004, 368, 56.
- [20] M. Selvakumar, P. Chandrasekar, M. Mohanraj, B. Ravisankar, J. Balaraju, Mater. Lett. 2015, 144, 58.
- [21] F. Makau, K. Morsi, N. Gude, R. Alvarez, M. Sussman, K. May-Newman, ISRN Biomater. 2013.
- [22] K. Morsi, V. Patel, J. Mater. Sci. 2007, 42, 2037.
- [23] A. Nikolaev, K. Ramazanov, A. Nazarov, V. Mukhamadeev, E. Zagibalova, E. Astafurova, J. Compos. Sci. 2023, 7, 271.
- [24] E. Dolgun, E. Zemlyakov, S. Shalnova, M. Guschina, V. Promahov, Mater. Today Proc. 2020, 30, 688.
- [25] TIMET, TIMETAL-64 2023, https://www.timet.com/assets/local/documents/technicalmanuals/TIMETAL\_6-4\_Properties.pdf (accessed: January 2024).
- [26] TIMET, TIMETAL-811 2023, https://www.timet.com/assets/local/documents/datasheets/alphaalloys/811.pdf (accessed January 2024).
- [27] G. Muvvala, D. Karmakar, A. Nath, Mater. Des. 2017, 121, 310.
- [28] C. Hong, D. Gu, D. Dai, A. Gasser, A. Weisheit, I. Kelbassa, M. Zhong, R. Proprawe, Opt. Laser Technol. 2013, 54, 98.
- [29] H. Tsuda, T. Ozaki, S. Mori, Mater. Trans. 2020, 61, 1090.
- [30] D. Gu, Y. Hagedorn, W. Meiners, K. Wissenbach, R. Proprawe, Compos. Sci. Technol. 2011, 71, 1612.
- [31] S. Liu, Y. Shin, Mater. Des. 2017, 136, 185.
- [32] E. Borisov, D. Masaylo, P. Vera, Key Eng. Mater. 2019, 822, 575.
- [33] M. Tang, L. Zhang, N. Zhang, Mater. Sci. Eng. A 2021, 814.
- [34] M. Burtscher, K. Kirchheimer, K. Weißensteiner, C. Bernhard, B. Lederhaas, T. Klein, S. Mayer, H. Clemens, *Pract. Metallogr.* 2018, 55, 693.
- [35] H. Okamoto, J. Phase Equilib. Diffus. 2006, 27, 306.
- [36] T. Gofrey, P. Goodwin, C. Ward-Close, Adv. Eng. Mater. 2000,
- [37] G. Hollenberg, G. Walther, J. Am. Ceram. Soc. 1980, 63, 610.